Available online at www.sciencedirect.com

ScienceDirect

journal homepage: www.elsevier.com/locate/he

Hydrogen production by glycerol steam reforming: How Mg doping affects the catalytic behaviour of Ni/Al_2O_3 catalysts

M.L. Dieuzeide [a], M. Laborde [a], N. Amadeo [a,*], C. Cannilla [b], G. Bonura [b], F. Frusteri [b]

[a] ITHES – CONICET-Universidad de Buenos Aires-Pabellón de Industrias, Ciudad Universitaria, 1428, Buenos Aires, Argentina

[b] National Council of Research, CNR-ITAE – Via S. Lucia 5, 98126, Messina, Italy

ARTICLE INFO

Article history:
Received 1 May 2015
Received in revised form
10 October 2015
Accepted 6 December 2015
Available online 28 December 2015

Keywords:
Glycerol steam reforming
Ni–Mg catalysts
Hydrogen production

ABSTRACT

Glycerol steam reforming, using Mg doped Ni/Al_2O_3 catalysts, was investigated with the aim to efficiently produce hydrogen. Catalyst containing different Mg loading were prepared by impregnation method maintaining constant the Ni loading (10 wt.%). Catalytic experiments were performed in fixed bed reactor operated at 500 and 600 °C. Characterization results revealed that Mg, further to infer a basic character to the carrier, promotes the Ni dispersion. In addition to observe that the catalytic activity was mainly dependent upon the Ni dispersion, the amount and morphology of coke formed during reaction was affected by Mg loading. In particular, the addition of 3wt% of Mg contributes to reduce the coke formation rate while a subsequent addition of Mg up to 10wt%, does not significantly affect neither the catalytic activity nor the carbon formation. By operating at 600 °C and with H_2O/Gly ratio of 6, low amount of coke, mainly of filamentous nature, was formed. The size and structure of carbon filaments changed as a function of Ni particle size and Mg loading.

Introduction

Vehicular transport is nowadays responsible for a large part of CO_2 emissions. Among the mitigation strategies, the Panel on Climate Change (IPPC) proposes the use of biofuels, electricity and hydrogen to reduce the transport greenhouse gases emissions [1].

Among the biofuels one of the most promising is biodiesel, which production has grown sharply in recent years. In biodiesel plants, around 10 wt.% of the vegetable oil or animal fat is converted to glycerol as a by-product [2]. Of course, the excess of glycerol production has led to a drastic decrease in its commercial value. Moreover, this non-toxic biomass has quite safe storage and handling policies. Such an integrated bioenergy production model may indeed allow a sustainable environmental local development [3].

Among different approaches proposed, the production of hydrogen by reforming processes has received particular attention [4–12].

* Corresponding author.
E-mail address: norma@di.fcen.uba.ar (N. Amadeo).
http://dx.doi.org/10.1016/j.ijhydene.2015.12.009

The steam reforming of glycerol (GSR) is an endothermic process that takes place according to the following main reaction scheme:

$$C_3H_8O_3 + 3H_2O \rightarrow 7H_2 + 3CO_2 \quad \text{(Glycerol steam reforming)} \tag{1}$$

$$C_3H_8O_3 \rightarrow 4H_2 + 3CO \quad \text{(Direct decomposition)} \tag{2}$$

$$CO + H_2O \rightarrow H_2 + CO_2 \quad \text{(WGS)} \tag{3}$$

$$3H_2 + CO \rightarrow CH_4 + H_2O \quad \text{(Methanation reaction)} \tag{4}$$

$$2CO \rightarrow CO_2 + C \quad \text{(Bouduard reaction)} \tag{5}$$

$$CH_4 \rightarrow 2H_2 + C \quad \text{(Methane decomposition)} \tag{6}$$

$$CO + H_2 \rightarrow H_2O + C \quad \text{(Coke deposition)} \tag{7}$$

However, the GSR process involves multiple complex reactions, which lead to several intermediate by-products that strongly affect H_2 selectivity.

H_2 selectivity is mainly the result of simultaneous glycerol decomposition (Eq. (2)) and water-gas shift (Eq. (3)) reactions, methanation reaction (Eq. (4)), and a series of reactions that lead to carbon formation (Eqs. (5)–(7)). A previous thermodynamic study [5] concluded that, in order to both favour H_2 production and minimize carbon formation, the steam reforming of glycerol should be performed at high temperatures and at atmospheric pressure with high water to glycerol molar feed ratio.

Besides reaction conditions, the catalyst also plays a key role on determining the reaction pathway and product distribution. In this sense, the fundamental steps involving the catalyst are the cleavage of C–C, O–H and C–H bonds of glycerol molecule while keeping the C–O ones [6–8].

Noble metal based catalysts are commonly used for the steam reforming reaction of hydrocarbons or alcohols [9–11] since they are highly active, and less susceptible to promote undesired carbon formation. On the other hand, catalysts based on non-noble transition metals are far cheaper, present higher availability than the former, but they are affected by coke formation. Among them, Ni based catalysts, in particular, are known to be active for the cleavage of C–C, O–H and C–H hydrocarbon bonds, while they also catalyse water gas shift reaction to remove CO adsorbed on metallic surface [6,12,13].

Several studies have been published regarding steam reforming of glycerol over Ni based catalysts [6,12,14–19]. Adhikari et al. [6] reported a glycerol conversion of 100% and a hydrogen yield of 57% over Ni/MgO catalysts at 650 °C. Additionally Thyssen et al. [18] obtained a glycerol conversion of 100% and a hydrogen yield of 54% referred to the stoichiometric one at 600 °C, over NiLaSi catalysts. Finally, Bobadilla et al. [19] studied glycerol steam reforming over NiSn/MgAl catalysts at 650 °C, they reported a glycerol conversion of 90% with a hydrogen yield of 45% of the stoichiometric one.

Regarding the catalyst support, it has been observed that supports featuring a basic character provide both higher activity and deactivation resistance [14–17,20–24]. The nature of the support influences the catalytic performance of supported Ni catalyst for the hydrocarbon reactions [25], since it affects metallic dispersion and stability.

Alumina-based support is normally used to prepare steam reforming catalyst due to its mechanical and chemical resistance. Nevertheless, the acid sites of alumina promote the deposition of carbon with negative consequence on catalyst stability and reaction pressure. One possible strategy to avoid carbon deposition is to favour its gasification by modifying the support with alkaline earth oxides such as MgO or CaO [25,26]. These additives favour water adsorption and OH surface mobility, decreasing the rate of coke deposition on catalyst surface [24].

It is known that hydrocarbons dissociate on the metal surface producing adsorbed carbon than can be either gasified to produce carbon oxides or polymerised to give rise to the formation of carbon species that accumulate on the metallic surface. Elementary carbon can also dissolve inside metal particle; in such case the carbon dissolution can lead to the formation of carbon with filamentous nature (whiskers). Or it can encapsulate the metallic particle and hence deactivates the catalyst [27].

In this paper the influence of Mg(II) doping on performance of Ni/Al_2O_3 catalyst in glycerol steam reforming reaction is investigated over a wide range of reaction conditions. Furthermore it is an aim of this work to understand the effect of Mg doping over carbon formation rate and carbon morphology.

Experimental

Catalysts preparation

The catalysts were prepared by the incipient wetness impregnation method. Aqueous solutions of $Mg(NO_3)_2 \cdot 6H_2O$ (99% Merck), with concentrations between 2.8 M and 14.0 M, and $Ni(NO_3)_2 \cdot 6H_2O$ (99% Merck) 3.9 M were prepared.

As elsewhere reported [28–30], bare γ-alumina (Rhône Poulenc, 200 m^2/g) was impregnated with increasing contents of Mg(II); the samples were dried in a furnace at 120 °C for 6 h, following by calcination at 900 °C for 6 h.

Then, each Mg(II)–Al(III) modified support and γ-Al_2O_3 calcined at 900 °C for 6 h, were impregnated with Ni(II) in order to reach a final loading of Ni(II) of 10wt.%. After impregnation with Ni(II) solution, the samples were dried at 120 °C for 6 h and calcined at 500 °C for 6 h.

Catalysts were identified as Ni(10)Mg(x)Al, being x the nominal content of Mg (wt.%) (0 wt.%, 3 wt.%, 5 wt.%, 10 wt.%).

Prior to impregnation with Mg(II) or Ni(II) solutions, bare γ-Al_2O_3 was crushed and sieved in order to obtain particles with diameters ranging between 44 and 125 μm.

Catalyst characterization

Fresh catalysts samples were characterized by N_2 adsorption – BET analysis, powder X-ray diffraction (PXRD), temperature programmed reduction (TPR), H_2 chemisorption and temperature programmed desorption of CO_2 (CO_2-TPD).

Used catalysts were characterized by temperature programmed oxidation (TPO), thermogravimetric analysis (TGA/

DSC), scanning electron microscopy (SEM), transmission electron microscopy assisted by EDAX.

Total surface area (BET) measurements

N_2-adsorption (BET) measurements were performed in a Micromeritics ASAP 2020 equipment. For each analysis, 100 mg of sample were employed. Before the analysis all the samples were outgassed under vacuum.

Powder X-rays diffraction (PXRD) measurements

Characterization by powder X-ray diffraction (PXRD) was performed with Siemens D5000 equipment, employing Cu Kα radiation.

Temperature programmed reduction (TPR)

Temperature programmed reduction (TPR) of the fresh samples was carried out in a Micromeritics Autochem II 2920, with a thermal conductivity detector (TCD). The sample (100 mg) was placed in a quartz U-shaped reactor. Before temperature programmed reduction, samples were pre-treated under Ar flow (50 mL/min) at 300 °C for 1 h. TPR was performed from 50 to 1000 °C at a heating rate of 10 °C/min, under a flow of 100 mL/min of 2%H_2/Ar mixture. Hydrogen consumption was followed by a TCD detector and estimated by the integration of peaks. From the TPR profiles of the fresh samples, it was estimated that more than 95% of Ni species was reduced.

H_2-chemisorption measurements

Metallic surface area and dispersion were obtained by means of H_2 chemisorption measurements carried out using Micromeritics Autochem II 2920 equipment. The sample (50 mg) was placed in a quartz U-shaped reactor, and reduced at 700 °C for an hour under a flow of 100 mL/min of (50:50) H_2/Ar mixture. The hydrogen chemisorption was performed at 25 °C (keeping this temperature by a N_2 flow, which has been previously cooled in a liquid nitrogen bath) by pulses of a mixture of H_2 (10%)/Ar in a flow of 100 mL/min of Ar. The metallic area of Ni was estimated assuming a $Ni_{surface}/H = 1$ stoichiometry and considering that an atom of Ni occupies 6.49 Å.

Thermogravimetric analysis (TGA)

The thermogravimetric differential scanning calorimetry (TG-DSC) analysis was performed by using a thermo-balance NETZSCH STA 409 instrument. The analyses were carried out with a heating rate of 10 °C min^{-1} from 20 to 920 °C in static air atmosphere.

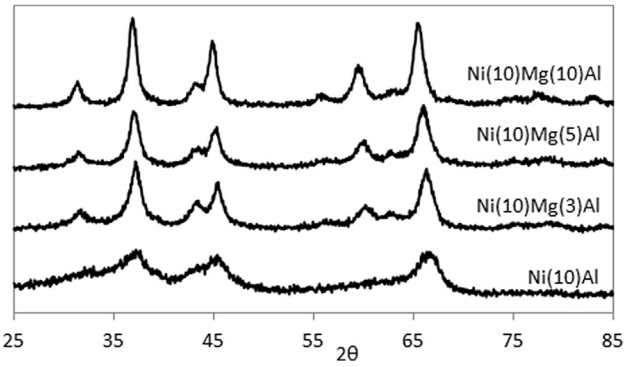

Fig. 1 – DRX diffractogram for Ni(10)Mg(x)Al with x = 0–10wt% [29].

Transmission electron microscopy assisted by EDAX

Carbon morphology structure was investigated by transmission electron microscopy (TEM) using a Philips CM12 microscope (resolution 0.2 nm), provided with high resolution camera, at an accelerating voltage of 120 kV. Suitable specimens for TEM analyses were prepared by ultrasonic dispersion in *i*-propylic alcohol adding a drop of the resultant suspension onto a holey carbon supported grid.

Catalysts testing

Catalytic tests were carried out in a stainless-steel continuous flow fixed bed reactor (Ø = 12 mm), at atmospheric pressure, heated with an electrical furnace equipped with temperature controllers. Experiments were carried out at a gas hourly space velocity (GHSV) of 0.95 min^{-1}; reaction temperatures ranging from 500 to 600 °C; water to glycerol molar ratio (H_2O/Gly) of 3.5:1 and 6:1 with a molar fraction of water in the feed of 60%. All catalytic tests were carried out using 440 mg of catalyst. Catalysts were reduced in situ under a flow of 100 mL/min of pure hydrogen with a heating ramp of 10 °C/min up to 700 °C, keeping the reactor at this temperature for one hour. Afterwards the catalyst temperature was set at the reaction temperature (500 °C or 600 °C) under a flow of N_2.

The liquid mixture containing water and glycerol was fed to the reactor by a HPLC pump and it was vaporized before to reach the catalytic bed. Both carrier gas (Ar) and reference one were fed by using mass flow controllers.

Moreover, in order to minimize mass transfer effect, catalysts particle size for all test were fixed between

Table 1 – BET surface area and H_2 chemisorption results [27].

Catalyst	BET (m^2/g)	Metal dispersion (%)	Metallic surface area (m^2/g sample)	Metallic surface area (m^2/g metal)	Cubic crystallite size (nm)
Ni(10)Al	80	1.50%	0.99	9.98	56.3
Ni(10)Mg(3)Al	90.6	2.75%	1.83	18.29	30.7
Ni(10)Mg(5)Al	77.9	2.31%	1.54	15.37	36.5
Ni(10)Mg(10)Al	73.1	2.06%	1.37	13.74	40.9

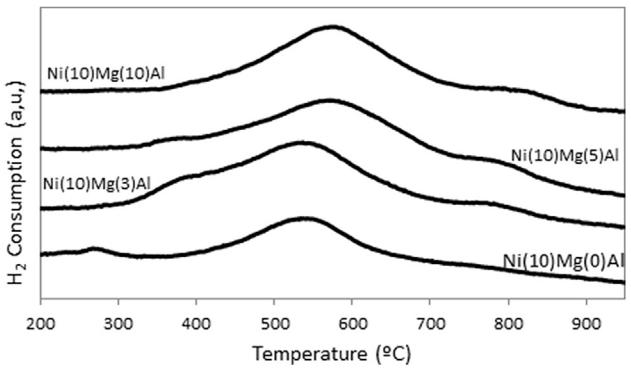

Fig. 2 – TPR profiles for Ni(10)Mg(x)Al catalysts with x = 0–10 wt.% [29].

44 μm < dp < 125 μm and total fed flow was higher than 200 mL/min.

Gaseous products were analysed on-line by TCD and FID detectors, in a GC chromatograph of Agilent Technologies (7890A). Liquid products were collected by condensation and analysed after four hours of reaction. Liquid products were only qualitative determined in order to identify the main products in the condensed stream: acetol, propilenglycol, ethilenglycol, ethanol and unreacted glycerol and water. A CarboxenTM 1010 Plot (30 m × 0.530 mm) column was employed to separate N_2, H_2, CO, CO_2 and CH_4; while a CP-PoraBOND Q (10 m × 0.32 mm) column was used to analyse the fed liquid mixture and the condensed mixture during the reaction.

- Glycerol conversion to gaseous products: $x_G = \sum \alpha_i F_i / 3F_{Gly}^{in}$
- Yield $Y_i = F_i / F_{Gly}^{in}$

Where F_{Gly}^{in} is the glycerol molar flow at the inlet, α_i are the number of C atoms in the product i molecule and F_i is the molar flow of gaseous product I formed from glycerol.

Results and discussion

Textural, structural and morphological properties

The XRD spectra of differently loaded Mg(II)–Ni catalysts, shown in Fig. 1, reveal the formation of stoichiometric $MgAl_2O_4$ phase (PDF 21-1152) and lines associated with NiO (PDF-65-2901). For Ni(10)Mg(0)Al catalyst reflections associated with NiO segregation at 2θ 37.25°, 43.35° and 62.85° (PDF-65-2901) and reflections associated with Al_2O_3 mainly at 67.5° (PDF-10-0425) were observed. As mentioned in previous paper [29], this result confirms that Ni(II) does not form Ni spinel like phases. For the catalysts promoted with Mg(II) the spinel reflection moves towards lower 2θ value as Mg content increases, which indicates the formation of Mg spinel-like phases. In addition, as previously published [29,30], spinel-like phase parameter cells were estimated based on peaks 400 and 440, in fact cell parameter continuously increased from Al_2O_3 parameter to the one corresponding to $MgAl_2O_4$. As regards the relative abundance of NiO phase respect to spinel-like phase, a constancy of the relative abundance of NiO was observed independently of Mg(II) content, which also suggested that NiO is not incorporated to spinel-like phase.

The textural properties of the catalysts with different Mg(II) contents are shown in Table 1. It can be observed that the catalyst with the support modified with 3wt% of Mg(II) presents the highest surface area, as well as the highest metallic area and dispersion and consequently the lowest particle size. In a previous work [29], it has been pointed out that the precoating of the support (Al_2O_3) with Mg (II) improves metal dispersion as well as stabilizes metal particles against sintering. Furthermore, the formation of Mg(II) spinel phase induces an improvement in the dispersion of metallic Ni. However, from these results it should be highlighted that the promotional effect of Mg (II) regarding metallic area and dispersion is more significant at lower contents of Mg(II).

This behaviour agrees with the results published by Iriondo [14], that at lower loadings of Mg(II) $MgAl_2O_4$ spinel phases are better dispersed, hindering Ni(0) particle diffusion and thus promoting higher stability.

In order to determine the reducible species present in each catalysts, TPR test were carried (Fig. 2). The TPR profiles are characterized by a preeminent broad peak centred in the range of 540–575 °C. For the catalyst without Mg(II) an additional small peak at 270 °C was observed. The temperature at the maximum of the reduction temperature signal increases from 540 °C to 575 °C as the loading of Mg(II) increases.

The de-convolution of reduction profiles put in evidence four main contributions, which are: i) NiO with weak interaction with the support at a reduction temperature of around 370 °C; ii) NiO with moderate interaction with the

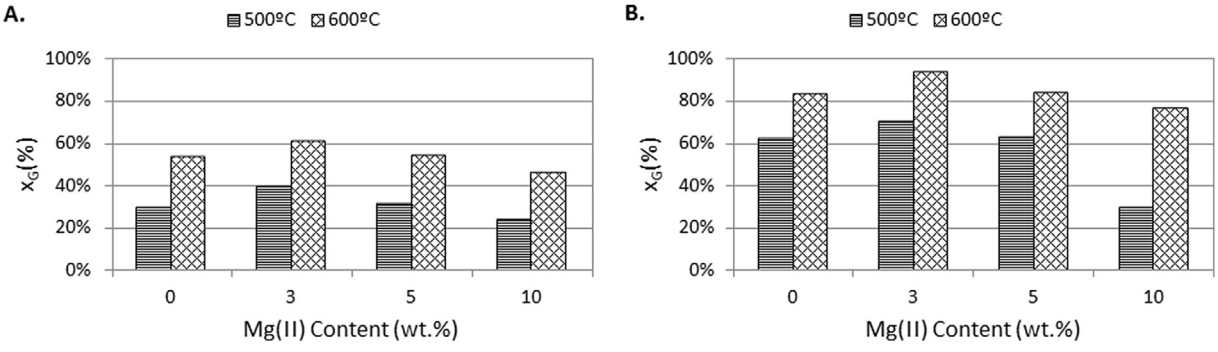

Fig. 3 – Glycerol conversion to gaseous products vs. Mg(II) content (wt.%) and reaction temperature (500 °C and 600 °C). A: R = 3.5:1. B: R = 6:1.

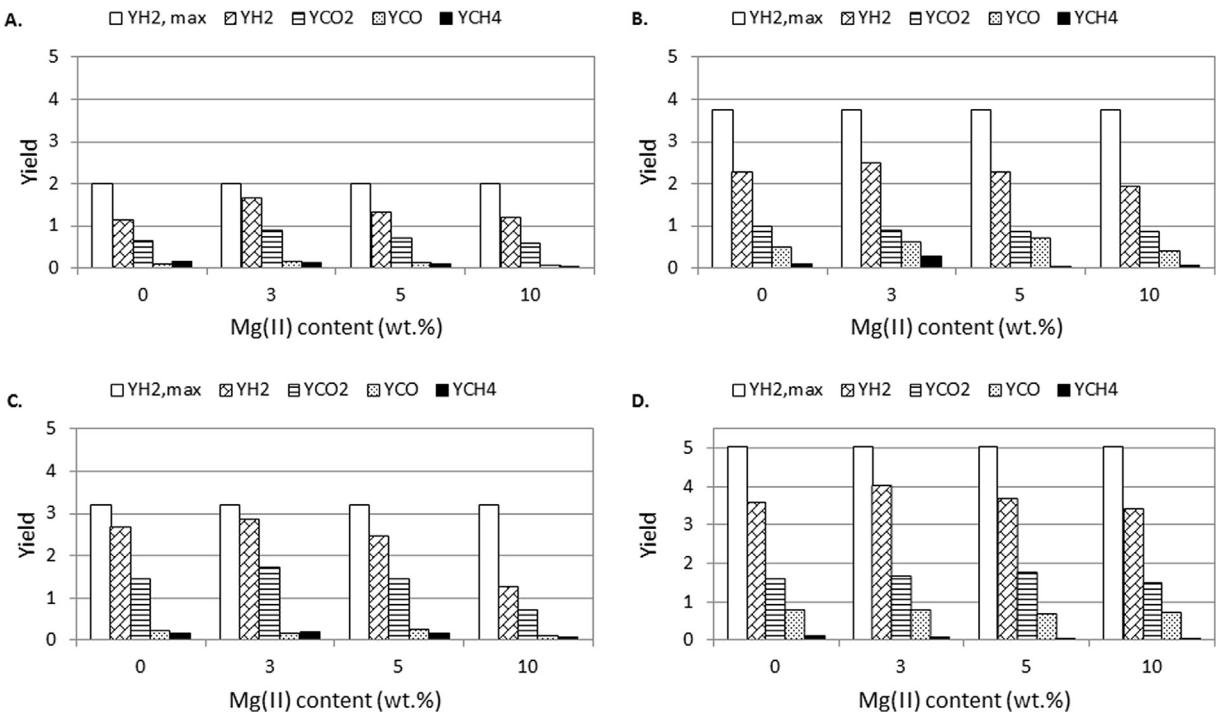

Fig. 4 – Yield to gaseous products vs. Mg(II) content (wt.%). A: R = 3.5:1 – T = 500 °C; B: R = 3.5:1 – T = 600 °C; C: R = 6:1 – T = 500 °C and D: R = 6:1 – T = 600 °C. YH_2, max is the thermodynamic hydrogen yield for each reaction condition.

support, centred at 550 °C, iii) non-stoichiometric $Ni_{1-x}Al_2O_{4-x}$ spinel at 750 °C and iv) stoichiometric Ni spinel at approximately 800 °C [14,20]. The predominant phase is, for all catalysts, NiO with moderate interaction with the support (about 80%). Particularly, for Ni(10)Mg(0)Al catalyst the mild signal obtained at 270 °C can be attributed to reduction of NiO isolated.

It is possible to distinguish that the temperature at the maximum of the reduction peak increased from 540 °C to 575 °C as Mg(II) content increases between 0 wt.% and 10wt.%. Since this reduction event is assigned to NiO with moderate interaction with the modified support, it would be possible to explain this increment in the reduction temperature as Mg (II) content increases, to a greater interaction between NiO and $MgAl_2O_4$.

Catalytic results

The catalytic results obtained by operating at different reaction temperature and molar ratio water to glycerol are shown in Figs. 3 and 4, in terms of glycerol conversion and products yield using different catalysts.

From Fig. 3 it emerges that regardless of the reaction temperature and the ratio H_2O/Gly employed, the conversion of glycerol follows a volcano-shaped trend: the best result was obtained with the catalyst containing 3wt% of Mg. As expected, at a higher temperature (600 °C) and with a ratio H_2O/Gly = 6, conversion of glycerol is higher, and in the case of the catalyst containing the 3wt% Mg it is close to 95%.

With regard to the gaseous products yield, Fig. 4 shows that, at 500 °C also using a ratio H_2O/Gly = 6, the hydrogen

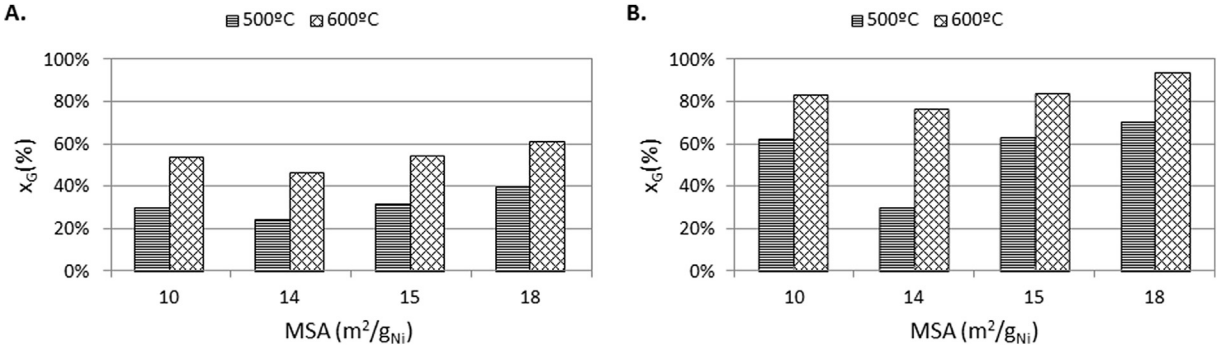

Fig. 5 – Glycerol conversion to gaseous products vs. Metallic surface area (MSA) and temperature (500 °C and 600 °C) A: R = 3.5:1; B: R = 6:1.

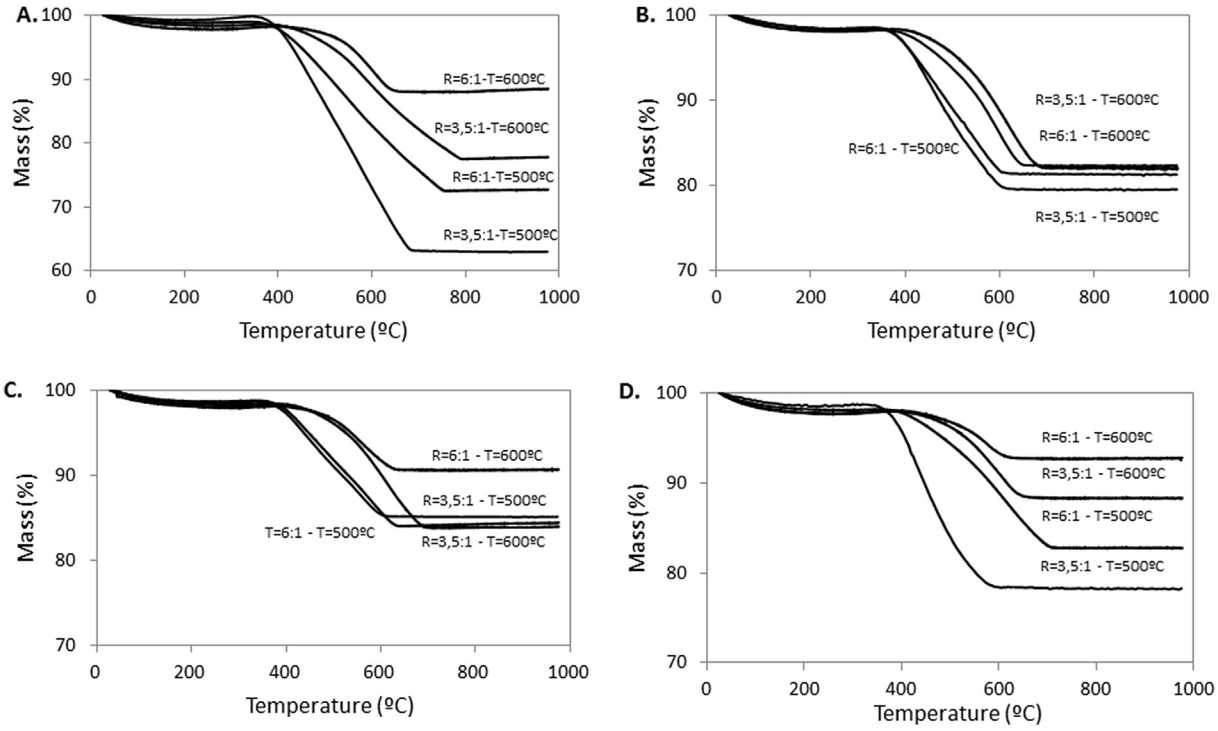

Fig. 6 – TGA profiles of used catalysts at different reaction conditions (Temperature and R). A: Ni(10)Mg(0)Al; B: Ni(10)Mg(3)Al; C: Ni(10)Mg(5)Al; D: Ni(10)Mg(10)Al.

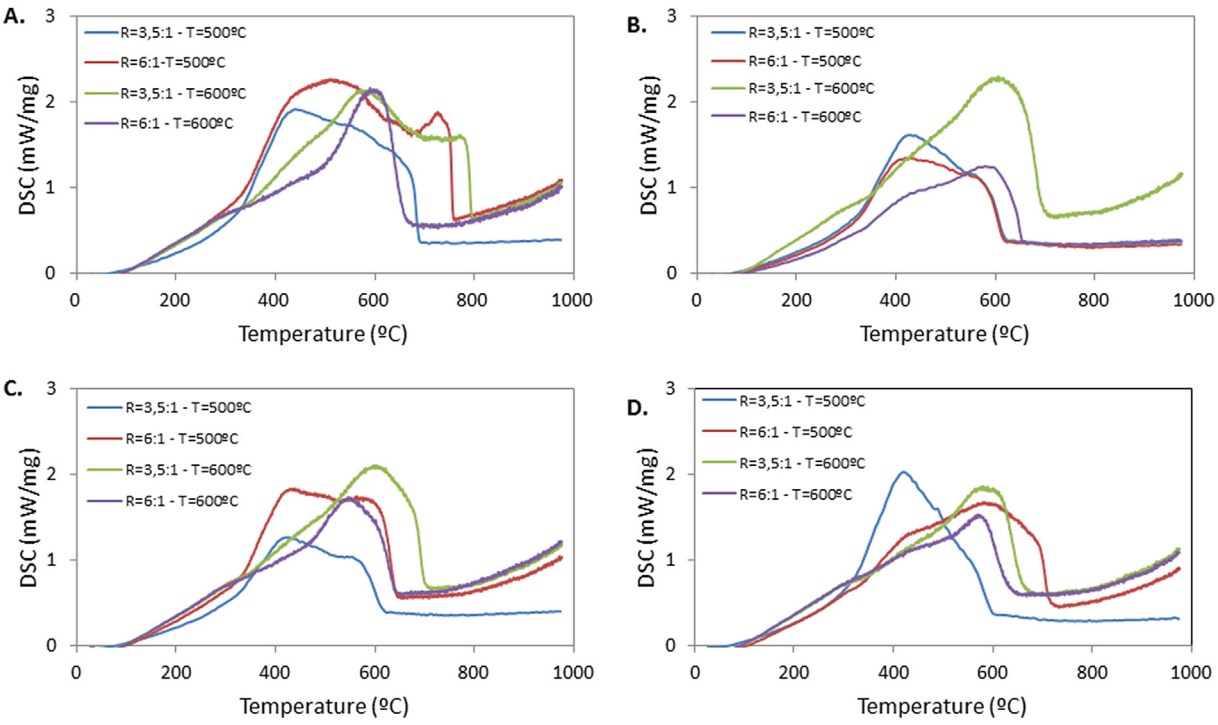

Fig. 7 – DSC profiles of used catalysts at different reaction conditions (Temperature and R). A: Ni(10)Mg(0)Al; B: Ni(10)Mg(3)Al; C: Ni(10)Mg(5)Al; D: Ni(10)Mg(10)Al.

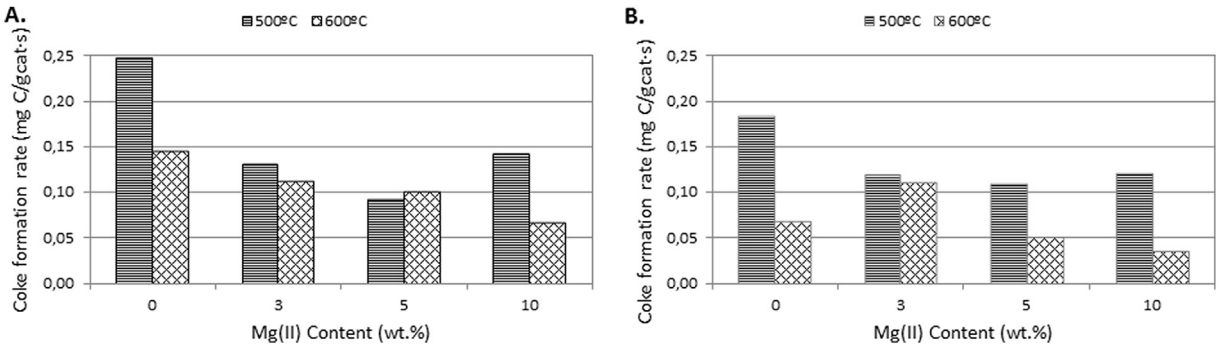

Fig. 8 – Carbon formation rate determined by TGA vs. Mg(II) content and temperature (500 °C and 600 °C). A: R = 3.5:1; B: R = 6:1.

yield never exceeds the value of 2.7 mol of H_2 produced per mole of glycerol fed (the stoichiometric value is 7 mol of hydrogen per mole of glycerol). As regards the yield of methane, which is considered an undesired product, it is noted that at 500 °C even operating with high H_2O/Gly ratio, the yield remains around 0.2. Naturally, increasing the reaction temperature to 600 °C the hydrogen yield grows significantly, and in particular at ratio of H_2O/Gly = 6, with the best catalyst (3wt% Mg), it reached a value close to 4 mol per mole of glycerol (around 80% of the hydrogen thermodynamic yield under these reaction conditions [5]). It can be also noted that at higher temperatures the yield of methane is lower and this can be correlated to the thermodynamic of methane steam reforming reaction which is favoured at high temperatures.

Even the ratio CO_2/CO, regulated by the WGS reaction, changes with temperature and the ratio H_2O/Gly, being 1.5 at 600 °C and ratio H_2O/Gly = 6.

By comparing the catalytic data with catalytic characterization data reported in Table 1, it can be deduced that the catalytic activity is closely related to the surface area of the metal Ni. In fact, the catalyst containing 3wt% Mg is characterized by a higher metal surface area respect to the other systems. Indirectly, this demonstrates that the presence of Mg, while being able to interact electronically with Ni, not significantly influences its catalytic behaviour. This hypothesis is confirmed by the data shown in Fig. 5. In fact, it can be observed that regardless of the temperature and the ratio H_2O/Gly used, the conversion of glycerol does not change significantly by using catalysts with different content of Mg and surface area.

Coke formation evaluation

As well known, one of the main problems in glycerol steam reforming is the coke formation [4] caused by the low thermal

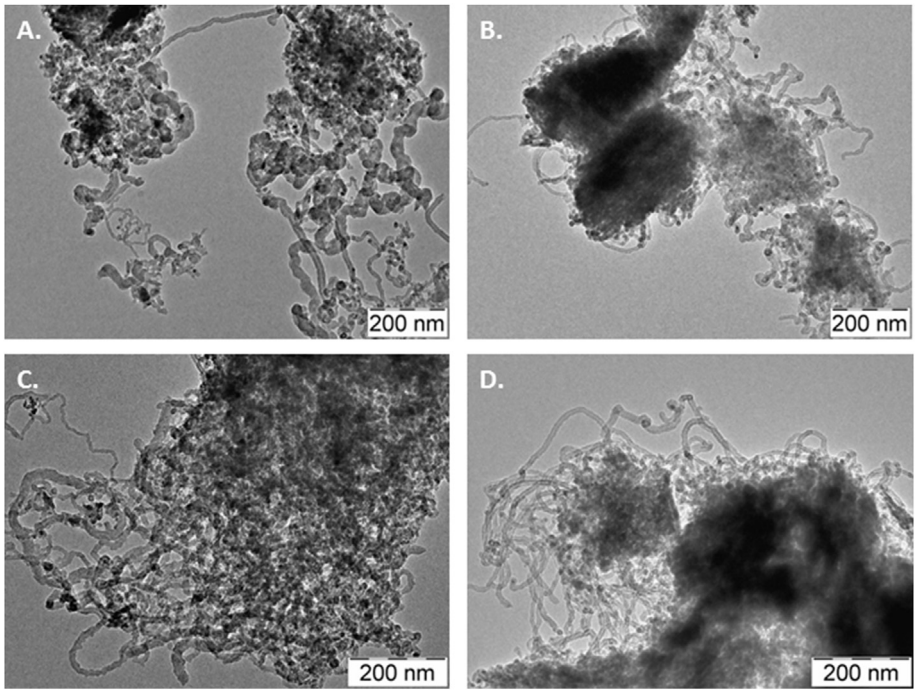

Fig. 9 – TEM of used catalysts at 500 °C and R = 3.5:1. A: Ni(10)Mg(0)Al; B: Ni(10)Mg(3)Al; C: Ni(10)Mg(5)Al; D: Ni(10)Mg(10)Al.

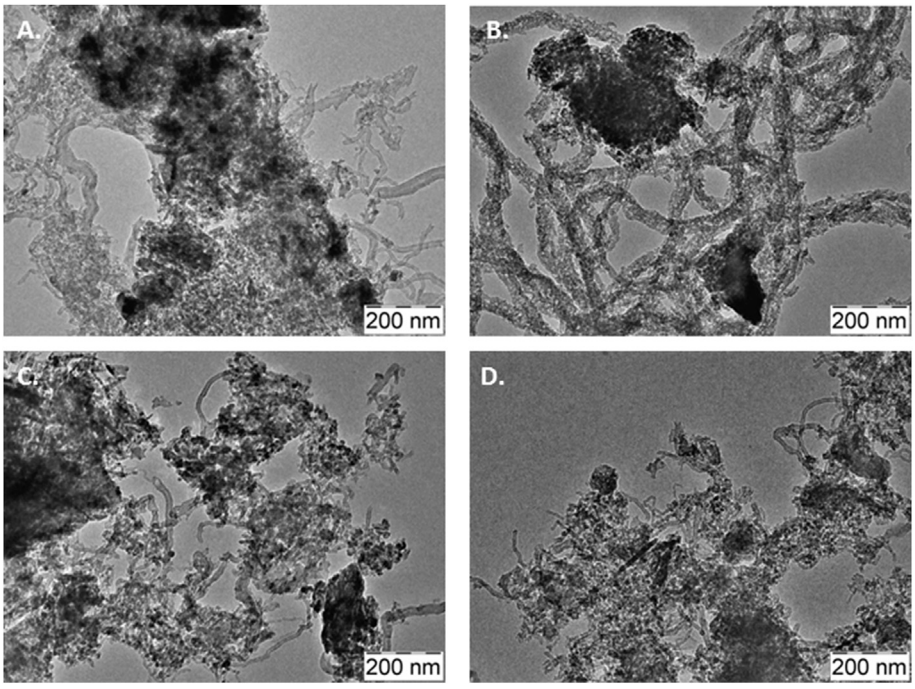

Fig. 10 – TEM of used catalysts at 600 °C and R = 3.5:1. A: Ni(10)Mg(0)Al; B: Ni(10)Mg(3)Al; C: Ni(10)Mg(5)Al; D: Ni(10)Mg(10)Al.

stability of glycerol. In fact, by operating at high temperature, glycerol can decompose in the empty zone of reactor, before to reach the catalyst surface [4]. Such decomposition can give rise to the formation of olefins that, as well known, are coke promoters mainly if the catalyst is characterized by acid properties [27].

Therefore, in order to investigate how carbon forms during reaction a series of characterization techniques have been employed to analyse the used catalysts.

In Fig. 6 the TGA profiles of catalysts tested at different reaction temperature and H_2O/Gly ratio are shown. The profiles of the free-Mg catalyst (Ni(10)Mg(0)Al), clearly evidence that the amount of coke formed strongly depends upon the reaction temperature and H_2O/Gly ratio. In the worst conditions, *i.e.* low temperature and low ratio H_2O/Gly, the loss in weight is almost 37%, while in the best conditions (high temperature and high ratio water-glycerol), the loss in weight is about three times lower (12%). This result clearly confirms what, already known, namely that increasing the reaction temperature and the partial pressure of water; coal gasification processes are favoured [5]. Adding Mg to the Ni catalyst, which causes both a decrease in the acidity of the surface [29] and an increase of the dispersion of the Ni (see Table 1), a significant difference in the coke formation is observable mainly at low reaction temperature (500 °C). This result can be justified considering that at low-temperature; carbonaceous species formed are more easily burnable as confirmed by DSC analysis shown in Fig. 7. From DSC profiles it can be observed that the isothermal peak maxima, associated to the combustion processes of carbon residues, fall to lower temperature (400 °C) in case the reaction is carried out at 500 °C; while by increasing the reaction temperature to 600 °C, the combustion peak shifts to 620 °C demonstrating so the formation of carbon species more difficult to be removed.

In order to better rationalize the results, TGA data have been elaborated in terms of coke formation rate as a function of reaction temperature and H_2O/Gly ratio. As shown in Fig. 8, the coke formation rate, referred to the Mg loading of Ni catalysts, does not follow a linear trend. In particular, at 500 °C and ratio H_2O/Gly = 3.5, a benefit was obtained up to a Mg(II) loading of 5wt%, after that the coke formation rate increase. At 600 °C, the coke formation rate decreases as the Mg loading increases but only in a slightly way.

As regard the nature of interaction of Mg with Ni, it has been reported that during calcination NiO–MgO solid solution can form and this strongly reflects on electronic properties of Ni at metallic state [31], practically its ability of C–H and C–C bonds cleavage is limited and all side reactions that lead to the formation of coke take place with lower rate. However, such phenomenon is more evident at low reaction temperature and low H_2O/Gly ratio, because as the reaction temperature and water partial pressure increase, the electronic effects become less important than kinetics associated to the coal gasification process [5].

From an accurate survey of TEM analysis on samples used in different reaction conditions, it was possible to make some considerations on the morphology and coke formation mechanism.

The TEM images of samples used at 500 °C, with a ratio H_2O/Gly equal to 3.5, are shown in Fig. 9. From a comparative evaluation of all images, regardless of the type of catalyst used (with or without Mg) the nature of the coke that forms is mainly of filamentous nature. In general, a homogeneity in terms of the diameter of the filaments (10–20 nm), closely

linked to the diameter of the Ni particles, can be observed. Unfortunately this evidence is associated with the type of mechanism of formation of the filament; in fact filament grows with the particle of Ni at the tip [32]. This phenomenon is well known and leads to the detachment of the metal particles from the surface of the support, with consequent deactivation of the catalyst. Under these reaction conditions, the variation of the Mg content of catalysts does not seem to influence in a significant way the differences in terms of the morphology of the filaments formed.

By, increasing the reaction temperature to 600 °C and keeping the ratio H_2O/Gly equal to 3.5 (see Fig. 10), a significant morphological difference of coke can be observed. First of all, the filaments are not as regular in shape and size. Multi-walled type filaments of size ranging between 10 and 50 nm are visible and they are not characterized by the presence of Ni at the tip. This suggests that by increasing the reaction temperature the coke formation mechanism changes and the metal particles are not detached from the surface of the support. In particular, using the catalyst containing 3% of Mg, it was observed a strange phenomenon. The filaments are highly irregular in structure. This demonstrated that they are not generated by the directly involvement of surface metal but rather they grow with mechanisms involving a surface containing both acid and base functionality. On catalyst containing only acid site (no Mg) or high loading of Mg (≥5%), then more basic, such filaments were not detected.

Conclusions

In this paper the behaviour of Ni supported on Mg-aluminate carrier containing different loading of Mg was investigated in the steam reforming of glycerol. Characterization results revealed that Mg plays a fundamental role in promoting both carrier basicity and Ni dispersion which positively reflects both on catalytic activity and carbon formation. In particular, an optimum of Mg loading (3wt%) enhanced the Ni dispersion from 1.50% to 2.75% and decreased the coke formation rate from 0.24 ($mg_C/g_{catalysts} \cdot s$) to 0.13 ($mg_C/g_{catalysts} \cdot s$) for 500 °C and R = 3.5.

The structure of carbon formed was affected both by Ni particle size and Mg presence. In particular the graphitization grade seems to increase as the Ni particle size decreases and Mg loading increases.

Acknowledgements

Authors would like to thanks to CONICET-CNR (Res. 351) for the financial support.

REFERENCES

[1] Ribeiro SK, Kobayashi S, Beuthe M, Gasca J, Greene D, Lee DS, et al. Transport and its infrastructure. In: Metz B, Davidson OR, Bosch PR, Dave R, Meyer LA, editors. Climate change 2007: mitigation. Contribution of working Group III to the Fourth Assessment Report of the Intergovernmental panel on climate change. Cambridge, United Kingdom and New York, NY, USA: Cambridge University Press; 2007.
[2] Vaidya PD, Rodrigues AD. Chem Eng Technol 2009;32:1463–9. http://dx.doi.org/10.1002/ceat.200900120.
[3] Franchini CA, Aranzaez W, Duarte de Farias AM, Pecchi G, Fraga MA. App Catal B Environ 2014;147:193–202. http://dx.doi.org/10.1016/j.apcatb.2013.08.036.
[4] Chiodo V, Freni S, Galvagno A, Mondello N, Frusteri F. Appl Catal A Gen 2010;381:1–7. http://dx.doi.org/10.1016/j.apcata.2010.03.039.
[5] Dieuzeide ML, Amadeo NE. Chem Eng Technol 2010;33(1):89–96. http://dx.doi.org/10.1002/ceat.200900260.
[6] Adhikari S, Fernando SD, Filip To SD, Bricka RM, Steele PH, Haryanto A. Energy Fuels 2008;22:1220–6. http://dx.doi.org/10.1021/ef700520f.
[7] Soares RR, Simonetti DA, Dumesic JA. Angew Chem Int Ed 2006;45:3982–5. http://dx.doi.org/10.1002./anie.200600212.
[8] Simonetti DA, Kunkes EL, Dumesic JA. J Catal 2007;247:298–306. http://dx.doi.org/10.1016/j.jcat.2007.01.022.
[9] Adhikari S, Fernando S, Haryanto A. Cat Today 2007;129:355–64. http://dx.doi.org/10.1016/j.cattod.2006.09.038.
[10] Czernik S, French R, Feik C, Chornet E. Ind Eng Chem Res 2002;41:4209–15. http://dx.doi.org/10.1021/ie020107q.
[11] Hirai T, Ikenaga N, Miyake T, Suzuki T. Energy Fuels 2005;19:1761–2. http://dx.doi.org/10.1021/ef050121q.
[12] Iriondo A, Barrio VL, Cambra JF, Arias PL, Guemez MB, Navarro RM, et al. Top Catal 2008;49:46–58. http://dx.doi.org/10.1007/s11244-008-9060-9.
[13] Aupretre F, Descorme C, Duprez D, Casanave D, Uzio DJ. J Catal 2005;233:464–77. http://dx.doi.org/10.1016/j.jcat.2005.05.007.
[14] Iriondo A, Guemez MB, Barrio VL, Cambra JF, Arias PL, Sánchez-Sánchez MC, et al. Scientific bases for the preparation of heterogeneous catalysts 175. Amsterdam: Elsevier; 2010. p. 449–52.
[15] Iriondo A, Barrio VL, Cambra JF, Arias PL, Guemez MB, Sanchez-Sanchez MC, et al. Int J Hydrogen Energy 2010;35:11622–33. http://dx.doi.org/10.1016/j.ijhydene.2010.05.105.
[16] Sánchez-Sánchez MC, Navarro RM, Fierro JLG. Int J Hydrogen Energy 2007;32:1462–71.
[17] Profeti LPR, Ticianelli EA, Assaf EM. Int J Hydrogen Energy 2009;34:5049–60. http://dx.doi.org/10.1016/j.ijhydene.2009.03.050.
[18] Thyseen VV, Maia TA, Assaf EM. Fuel 2013;105:356–63. http://dx.doi.org/10.1016/j.fuel.2012.06.105.
[19] Bobadilla LF, Penkova A, Romero-Sarria F, Centeno MA, Odriozola JA. Int J Hydrogen 2014;39:5704–12. http://dx.doi.org/10.1016/j.ijhydene.2014.01.136.
[20] Young Koo K, Roh HS, Taek Seo Y, Joo Seo D, Lai Yoon W, Bin Park S. Appl Catal A Gen 2008;340:183–90. http://dx.doi.org/10.1016/j.apcata.2008.02.009.
[21] Cheng Z, Wu Q, Li J, Zhu Q. Catal Today 1996;30:147–55. http://dx.doi.org/10.1016/0920-5861(95http://dx.doi.org/10.1016/0920-5861(95)00005-4.
[22] Wang S, Lu GQJ. Chem Technol Biotechnol 2000;75:589–95. http://dx.doi.org/10.1002/1097-4660(200007)75:7.
[23] Basagiannis AC, Verykios XE. Catal Today 2007;127:256–64. http://dx.doi.org/10.1016/j.cattod.2007.03.025.
[24] Rostrup-Nielsen JR, Sehested J, Norskov JK. Adv Catal 2002;47:65–139. http://dx.doi.org/10.1016/S0360-0564(02http://dx.doi.org/10.1016/S0360-0564(02)47006-X.
[25] Frusteri F, Italiano G, Espro C, Cannilla G, Bonura G. Int J Hydrogen Energy 2012;37:16367–74. http://dx.doi.org/10.1016/j.ijhydene.2012.02.192.

[26] Horiuchi T, Sakuma K, Fukui T, Kubo Y, Osaki T, Mori T. App Catal A General 1996;144:111–20. http://dx.doi.org/10.1016/0926-860X(96http://dx.doi.org/10.1016/0926-860X(96)00100-7.
[27] Trimm DL. Poisoning of metallic catalysts. In: Deactivation and poisoning of catalysts. Marcel Dekker Inc.; 1985. p. 151–84.
[28] Dieuzeide ML, Iannibelli V, Jobbagy M, Amadeo N. Int J Hydrogen Energy 2012;37:14926–30. http://dx.doi.org/10.1016/j.ijhydene.2011.12.086.
[29] Dieuzeide ML, Jobbagy M, Amadeo N. Catal Today 2013;213:50–7. http://dx.doi.org/10.1016/j.cattod.2013.02.015.
[30] Dieuzeide ML, Jobbagy M, Amadeo N. Int J Hydrogen Energy 2014;39:16976–82. http://dx.doi.org/10.1016/j.ijhydene.2014.08.097.
[31] Young Koo K, Roh H, Jung U, Joo Seo D, Lai Yoon W. Catal Today 2009;146:166–71. http://dx.doi.org/10.1016/j.cattod.2009.02.002.
[32] Li Y, Li D, Wang G. Catal Today 2011;162:1–48. http://dx.doi.org/10.1016/j.cattod.2010.12.042.